Proceedings of the XIII International Conference "Ion Implantation and Other Applications of Ions and Electrons"

Thermal Desorption of Kr Implanted into Germanium

M. Turek[a,*], A. Droździel[a], K. Pyszniak[a], S. Prucnal[a], J. Żuk[a] and P. Węgierek[b]

[a] *Institute of Physics, Maria Curie-Skłodowska University in Lublin, Pl. M. Curie-Skłodowskiej 1, 20-031 Lublin, Poland*
[b] *Faculty of Electrical Engineering and Computer Science, Lublin University of Technology, Nadbystrzycka 38A, 20-618 Lublin, Poland*

Doi: 10.12693/APhysPolA.142.776 *e-mail: mturek@kft.umcs.lublin.pl

Thermal desorption spectrometry measurements of Kr implanted with energies 100 keV and 150 keV (fluence 2×10^{16} cm^{-2}) into the Ge sample are considered. A sudden release of Kr is observed in the temperature range of 800–840 K. The very narrow peaks in the thermal desorption spectrometry spectra (width of several K) come most probably from the release of gas trapped in pressurized bubbles. Analysis of peak shifts with increasing heating rate enabled the estimation of the adsorption activation energy values of 2.5 eV and 2.3 eV for the implantation energies 100 keV and 150 keV, respectively. These values are comparable to those obtained for Ar implanted into the Ge samples and for Kr implanted into the Si samples.

topics: thermal desorption spectroscopy, ion implantation

1. Introduction

Thermal desorption spectroscopy (TDS), sometimes also known as thermal programming desorption (TPD), is a very common method to study adsorption, desorption, as well as the reaction of adsorbed particles on surfaces. The cornerstone of the method is measuring the desorption rate of released gases from the surfaces as a function of the surface temperature. Keeping in mind that adsorbates with a higher energetic barrier undergo desorption at a higher temperature, and the fact that adsorbates release depends on heating speed, one can determine, e.g., desorption activation energies of adsorbates [1]. A detailed analysis of the TDS spectra of gases introduced (e.g., by ion implantation) into the solid target provides information concerning the interactions of the dopant with the lattice and defects within it, as well as about the diffusion process [2]. Thermal desorption spectroscopy is often used not only to study disorder in crystalline targets due to the ion bombardment but also to investigate the retention of impurities in the materials typically used in both a "classical" (fission) and future fusion nuclear reactors, i.e., tungsten [3, 4], graphite [5, 6] or beryllium [7, 8] and other plasma-facing materials. It should be mentioned that TDS is often combined with positron annihilation techniques in order to get a deeper insight into the structure of defected layers [3, 9–11]. The gas-charged layer can either be a natural one (e.g., oxide layer) or prepared by ion implantation or magnetic sputtering in a specific atmosphere [12].

One should keep in mind that not only reactor materials containing gas-filled cavities or bubbles are studied with TDS, but also other metals [13, 14] thin layers [15, 16] and semiconductors, including the most important material for the microelectronic industry — silicon, because the bubble formation can be essential for the Smart-cut processing [17] as well as for gettering of impurities [18, 19]. The fabrication of helium bubbles in Si by ion implantation (mainly characterised by large fluence, i.e., of the order 10^{16} cm^{-2}) has attracted the attention of several scientific groups [20–25], altering the implantation energy in the range from 10 keV to several MeV, as well as other parameters like fluence, implantation, and annealing temperatures etc. Also, the release of other inert gases (including Ar [26–29], Xe [30–32], and Kr [33]) implanted in a wide spectrum of energy was investigated over the years, showing that desorption activation energies are usually higher for gases with larger atomic radii.

Germanium is characterized by much higher carrier mobility ($\simeq$ 3900 cm^2/(V s) for electrons and $\simeq$ 1900 cm^2/(V s) for holes) than Si, so nowadays it attracts the attention of scientists and engineers as a candidate for a material, which enables significant improvement of the performance of microelectronic and optoelectronic devices. Moreover, the

close similarity of Si and Ge [34] could make easier the integration of that material with contemporary CMOS technology. It was recently demonstrated that pure germanium (a material characterized by an indirect bandgap) could be transformed into a semiconductor with a direct bandgap using Sn doping and P hyperdoping followed by millisecond annealing, which also resulted in an even further enhancement of carrier mobility [35–38].

Production of layers containing numerous gas bubbles in Ge or in thin layers of Ge on the insulator could be a crucial step toward developing a Smart-cut analogue for this material class. It was shown that bubbles with a diameter of $\simeq$ 1 nm were formed due to a 60 keV He irradiation with the fluence of 2×10^{16} cm^{-2} [39]. It is also known that intense (of the order 10^{17} cm^{-2}) irradiation with H^+ ions followed by annealing at 200–350°C leads to blistering of the Ge surface [40], as well as the blister transformation into the craters for higher irradiation fluence. In our previous papers, we studied the thermal desorption of He [41] and Ar [42] implanted into Ge samples with the fluence 1×10^{16} cm^{-2} and 2×10^{16} cm^{-2}, respectively. No signs of surface blistering or crater formation was observed in these cases. Desorption activation energies were close to 0.75 eV in the case of He (100 keV), while much higher value ($\simeq$ 3.2 eV) was found for Ar implanted with the same energy. It should be mentioned here that the spectra of He were very broad ($\simeq$ 200 K full width at half maximum (FWHM), much broader than in the case of the release from Si [25]) in the range of 600–900 K, while the Ar release was rather sudden, in the form of single sharp peaks (in the range 790–840 K). A sudden release may be the result of an increase of gas pressure inside the cavities formed by the coalescence of vacancies above some critical value.

The paper presents the investigations of thermal desorption of heavier inert gas, which is krypton implanted into a Ge target with the energies 100 keV and 150 keV, in order to determine changes of the desorption activation energy with the gas projectile mass (and atomic radius), as well as to examine possible changes of Ge surface morphology after releasing the gas. The implantation fluence was kept the same as in the previous case of Ar (i.e., 2×10^{16} cm^{-2}). Thermal desorption spectra were collected for linear heating profiles with the ramp rates ranging from 0.35 up to 2 K/s. Analysis of the sudden Kr release peak with the ramp rate was performed to estimate the desorption activation energy. The results are discussed and compared to those obtained for lighter gases. A short description of the experimental setup is added for completeness.

2. Experimental setup

Ge samples (orientation 110) were irradiated with Kr^+ ions with energies 150 keV and 100 keV. The implantation fluence was set to 2×10^{16} cm^{-2} as in the previously considered case of Ar [42]. Implantation was performed at room temperature. The implantation current density was kept below 1 μA/cm^2 in order to prevent excessive sample heating and sputtering.

The thermal desorption spectrometer used for the measurements was described in detail in previous papers [25, 29, 32, 33]. The brief description is given for completeness and also due to the fact that the setup is constantly being developed in search for better performance. The main body of the equipment is a stainless steel vacuum chamber equipped with numerous flanges and ports. It contains a sample holder connected to the Boralectric HTR1002 (Momentive, Strongsville OH, USA) heater. The holder–heater block is shielded by steel and molybdenum sheets in order to prevent excessive heating of the chassis and to limit the precipitation of vapours coming out of the sample on its internal surfaces. The heater is powered by a programmable power supply EA-PS 8080T (EA-Electro-Automatik GmbH, Viersen, Germany), more powerful than the previously used unit, which enables fast and reliable heating with different profiles and rates up to $\simeq$ 1600 K (this upper limit is determined mainly by the fact that the temperature is measured using a K-type thermocouple). The thermocouple and power supply are connected (via Hewlett-Packard 34970A data acquisition switch) to the personal computer (PC) controlling the experimental setup. The power supply is controlled by custom-made software based on the proportional–integral–derivative (PID) algorithm. During all presented measurements, there was deployed the linear profile of the sample heating

$$T(t) = T_o + \beta t, \tag{1}$$

where T_o is the initial (room) temperature and β is the heating ramp rate (usually in the range 0.35–2 K/s).

The partial pressure of the selected (implanted) isotope(s) is measured by a quadruple mass spectrometer QMG 220 M (Pfeiffer Vacuum, Asslar, Germany) with a secondary electron multiplier detector in order to enhance the detection threshold compared to the early version of the setup. The spectrometer is controlled by the Quadera™software package, which also enables saving and analyzing the spectra.

The vacuum system in its present form is compound of two independent turbomolecular and rotary vane vacuum pumps — one providing vacuum condition in the main vessel, the other in the mass spectrometer compartment. These two parts of the TDS spectrometer can be separated using the gate valve system when necessary, e.g., during heater annealing. The two pump sets allow achieving the pressure of 10^{-8} mbar during the idle run of the TDS spectrometer. Closing the gate valve no. 10 in the measurement phase directs the gases emitted

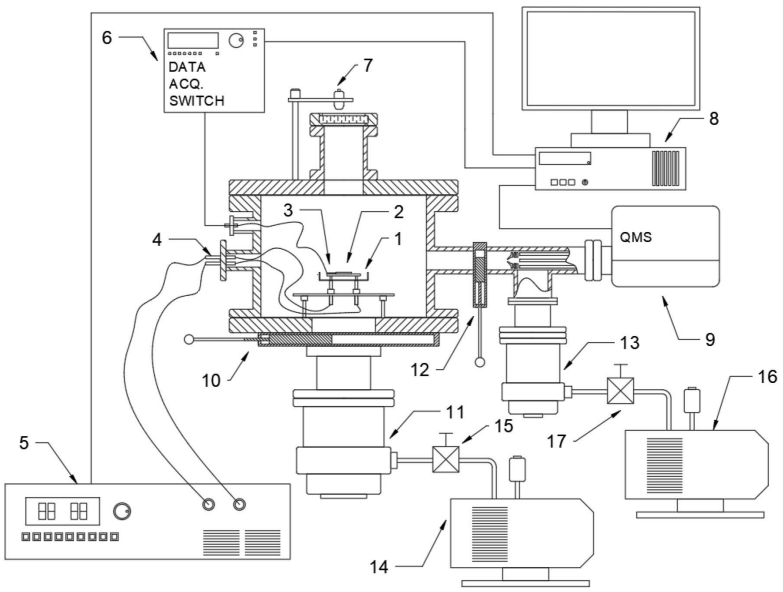

Fig. 1. Schematic drawing of the experimental setup: 1 — sample heater; 2 — sample; 3 — K-type thermocouple; 4 — electrical feedthrough; 5 — programmable power supply; 6 — data acquisition switch; 7 — pyrometer (optional); 8 — PC-class microcomputer; 9 — quadruple mass spectrometer; 10, 12 — gate valves; 11, 13 — turbomolecular pumps; 14, 16 — rotary vane forevacuum pumps; 15, 17 — forevacuum gate valves.

from the sample through the gate valve no. 12 toward the mass spectrometer (see Fig. 1), which enables the application of very small samples of a surface of 0.25 cm^2.

3. Results

The distributions of the implanted Kr in the sample and the produced damage (vacancy density) were calculated using the SRIM package. The results are presented in Fig. 2. The Kr^+ projected range was $R_p = 60$ nm with a straggling of 27 nm in the case of $E = 150$ keV, while for the lower energy $E = 100$ keV these magnitudes were 40 nm and 20 nm, respectively.

The projected ranges are almost an order of magnitude shorter than in the case of He implantation into Ge [41] and approximately two times shorter than in the previously considered case of Ar irradiations [42]. It should be noted that the concentrations of produced vacancies are also much higher, more than twice higher than the concentrations of Ar implanted into Ge. Moreover, the distribution of the vacancies differs much from that produced, e.g., by He implantations. In the case of He irradiation, one observes a disordered layer covered by a rather thick, rather unmodified layer, while in the case of the Kr bombardment, the vacancy distribution is rather shallow and reaches the sample surface.

These differences have some impact on the character of the He and Kr spectra. As it was already mentioned — the He spectra contained multiple, very broad peaks (their combined width was $\simeq 200$ K). The spectra registered for Kr are presented in Figs. 3 and 4. They contain very narrow

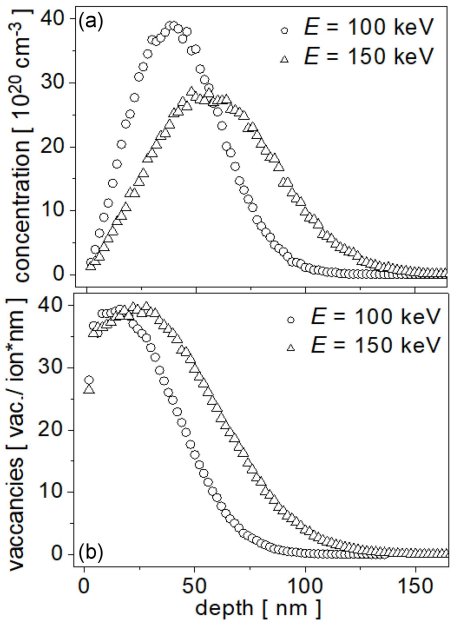

Fig. 2. Implanted He concentration (a) and vacancies distributions (b) in Ge calculated using SRIM code.

peaks (width of several K). The release of Kr from Ge samples is observed in the temperature range of 800–850 K, more or less the same as in the case of Ar measurements, and slightly lower compared to the He release in the case of 100 keV irradiation. As in the previous case of Ar implantation to Ge, measurements of the background spectra (i.e., measured without the implanted sample) were also performed.

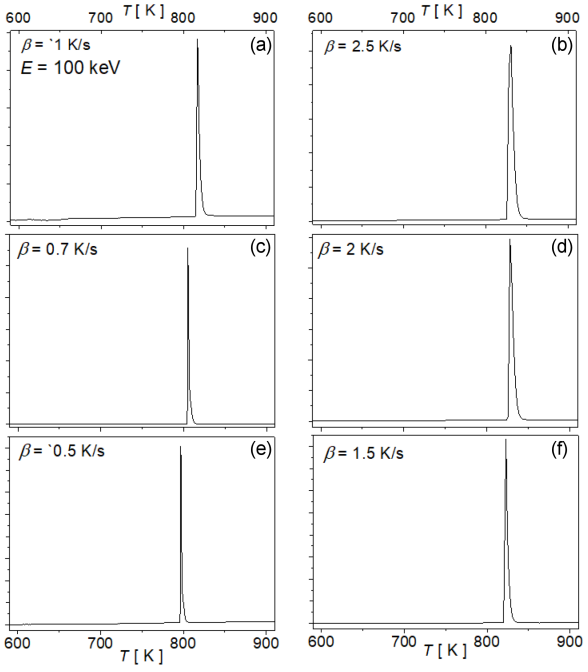

Fig. 3. TDS spectra collected for the 100 keV Kr^+ implanted samples.

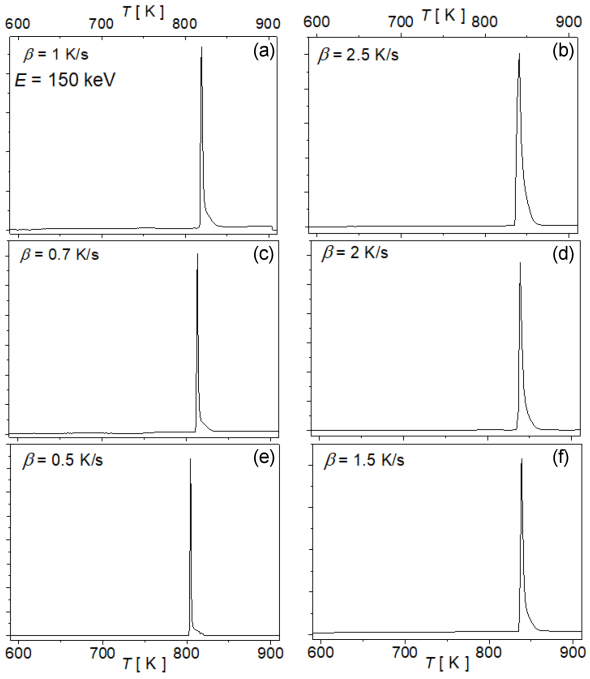

Fig. 4. TDS spectra collected for the 150 keV Kr^+ implanted samples.

An example is shown in Fig. 5. One has to keep in mind that the magnitude of the signal presented in Fig. 5 is enlarged by more than 2 orders of magnitude (compared to Figs. 3 and 4). The very weak Kr release, which starts just above 500 K (and is also observed in the TDS spectra of implanted samples), most probably comes from gas adsorbed on the internal surfaces of the sample holder, shield and the main chamber.

In the case of He implanted into Ge with the fluence 10^{16} cm^{-2}, it was assumed that the slow release of Ge is related to the diffusion of He atoms in interstitials, vacancies, as well as to those trapped in the He_nV_m clusters [21, 43]. Emission from the small gas-filled vacancy cluster could not be excluded, but the relatively low fluence seemed to be too low to lead to the creation of large pressurized bubbles. It should be reminded here that fluences above 3×10^{16} cm^{-2} were required in the case of H irradiation in order to create blisters. In the considered case, the fluences were higher than for He, and the projected ranges were shorter by an order of magnitude. This, combined with the higher concentration of produced vacancies, probably leads to easier formation of gas-filled bubbles. A sudden release of Kr is observed when the critical pressure is exceeded due to the increasing temperature of the sample, as it was in the case of Ar implanted into Ge [42] or heavy inert gases implanted into silicon [32, 33].

Looking at the spectra in Figs. 3 and 4, as well as at the data gathered in Table I, one can observe that the positions of the Kr release peaks are shifted towards higher temperatures as the heating ramp rate β increases. The shifts are comparable to those measured for Ar implanted into Ge, and much smaller than those observed for He (change of $\simeq 70$ K when β increased from 0.45 up to 1.5 K/s). As in the case of Ar release, the peaks obtained for the samples implanted with $E = 150$ keV and $E = 100$ keV are shifted by only several K, while in the case of implanted Si targets, these shifts even reached values of several hundreds of kelvins.

TABLE I

Temperatures of Kr release (corresponding to TDS spectra peaks) and desorption activation energies for two implantation energies.

E [keV]	β [K/s]	T_p [K]	Q [eV]
150	0.35	796	2.50 ± 0.15
	0.5	804	
	0.7	813	
	1	820	
	1.5	837	
	2	839	
	2.5	841	
100	0.5	797	2.30 ± 0.15
	0.7	805	
	1	816	
	1.5	823	
	2	828	
	2.5	832	

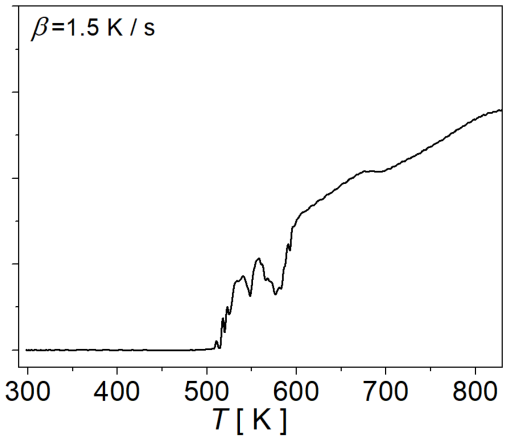

Fig. 5. Example of background TDS signal (without any sample).

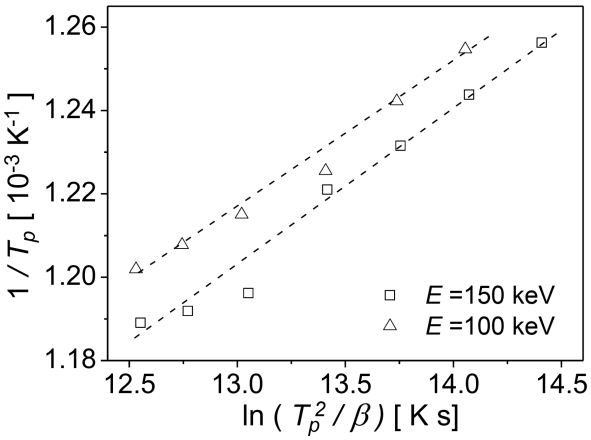

Fig. 6. Redhead's plots ($1/T_p$ vs $\ln(T_p^2/\beta)$) for Ge samples implanted with 100 keV and 150 keV Kr^+ ions.

The analysis of the peak shifts according to the Redhead's approach [44] enables estimation of the desorption activation energies. In the case of the first order process, the Polanyi–Wigner equation describing the desorption rate per unit surface has the form

$$\frac{\mathrm{d}n}{\mathrm{d}t} = -\gamma\, n \exp\left(-\frac{Q}{k_\mathrm{B}T}\right), \tag{2}$$

where n is the surface density of the desorbing substance, k_B is the Boltzmann constant, Q is the desorption activation energy and γ is a pre-exponential factor. Assuming that one deals with a linear heating profile described by (1) and denoting the temperature corresponding to the maximal release (peak of the TDS spectrum) as T_p, one obtains from the condition $\mathrm{d}^2n/\mathrm{d}t^2 = 0$ that

$$\frac{1}{T_p} = \frac{k_\mathrm{B}}{Q}\ln\left(\frac{T_p^2}{\beta}\right) + \frac{k_\mathrm{B}}{Q}\ln\left(\gamma\frac{k_\mathrm{B}}{Q}\right). \tag{3}$$

Consequently, the diffusion activation energy Q can be obtained by calculating the slope of the $1/T_p$ vs $\ln(T_p^2/\beta)$ plot. Such plots are presented in Fig. 6. One can see that the slopes of the straight lines fitted to the experimental points obtained for the two implantation energies are similar. Estimations of the desorption activation energy are presented also in Table I. The value of Q for $E = 100$ keV is approximately 2.5 eV and slightly lower (2.3 eV) for $E = 150$ keV. The estimation uncertainties are below 10% in both cases. The obtained values of Q are higher than those obtained for He implanted into Ge and comparable to that obtained in the case of Kr implantation to Si [31].

The fact that the desorption activation energy for Kr ($E = 100$ keV) is by 1 eV lower than the corresponding value for Ar is rather surprising in light of our previous results — an increase of Q with the atomic number (and atomic radius) of inert gases in the case of implantation to Si was observed [25, 29, 31, 32]. The lowering of the desorption activation energy may be due to the high amount of disorder introduced by more shallow (and higher fluence) implantations to Ge by heavier inert gases. It should be stressed that the release temperatures are not as close to the melting point as observed for the Si matrix. It remains an open question of whether similar behaviour is observed even for the heavier inert gas, namely Xe, or rather the release of such a heavy dopant requires larger temperatures, as it was observed for the implanted silicon.

4. Conclusions

The paper presents studies of thermal desorption of Kr implanted with energies of 100 keV and 150 keV into germanium. Thermal desorption spectra were collected during the sample heating with different ramp rates ranging from 0.5 up to 2.5 K/s. The release of the implanted Kr in the form of a single sharp peak was observed in the temperature range $\simeq$ 800–840 K, slightly lower than in the case of He implanted into Ge. This abrupt Kr emission (similar to that observed in the case of Ar implantation) is most probably the effect of a pressure increase above a critical threshold in the gas bubbles formed in the cavities formed due to the coalescence of vacancies and its clusters in the Ge matrix. A shift of the release peaks towards higher temperatures was observed with increasing heating ramp rate. Redhead analysis of the shift enabled estimation of the desorption activation energy values, i.e., 2.5 eV and 2.3 eV for implantation energies 100 keV and 150 keV, respectively. These values are comparable to those obtained for Ar implanted into the Ge and Si samples.

Acknowledgments

The research was co-funded by the grant of Polish National Science Center No. 2016/23/B/ST7/03451.

References

[1] S. Ogura, K. Fukutani in: *Compendium of Surface and Interface Analysis*, Springer, Singapore 2018.

[2] A.A. van Gorkum, E.V. Kornelsen, *Vacuum* **31**, 89 (1981).

[3] K. Sato, R. Tamiya, Q. Xu, H. Tsuchida, T. Yoshiie, *Nucl. Mater. Energy* **9**, 554 (2016).

[4] V.Kh. Alimov, B. Tyburska-Püschel, S. Lindig, Y. Hatano, M. Balden, J. Roth, K. Isobe, M. Matsuyama, T. Yamanishi, *J. Nucl. Mater.* **420**, 519 (2012).

[5] A. Kreter, M. Baldwin, R. Doerner, D. Nishijima, P. Petersson, A. Pospieszczyk, M. Rubel, K. Umstadter, *Phys. Scr.* **2009**, 014012 (2009).

[6] A.A. Airapetov, L.B. Begrambekov, S.V. Vergazov, A.A. Kuzmin, O.C. Fadina, P.A. Shigin, *J. Surf. Invest. X-ray* **4**, 567 (2010).

[7] M. Zibrov, Yu. Gasparyan, S. Ryabtsev, A. Pisarev, *Phys. Proc.* **71**, 83 (2015).

[8] Corregidor, I. Jepu, G.F. Matthews, A. Widdowson, *Fusion Eng. Design* **133**, 135 (2018).

[9] Z. Shen, L. Guo, W. Zhang, S. Jin, X. Cao, Y. Long, Y. Wei, *Materials* **1**, 1523 (2018).

[10] Z. Hu, Z. Li, Z. Zhou, C. Shi, H. Schut, K. Pappas, *J. Phys. Conf. Series* **505**, 012014 (2014).

[11] L. Chao-Zhuo Z. Zhu-Ying, S. Li-Qun, W. Bao-Yi, H. Xiao-Peng, Z. Guo-Qing *Chinese Phys. Lett.* **24,** 2357 (2007).

[12] L. Wang, T. Hao, B.-L. Zhao, T. Zhang, Q.-F. Fang, C.-S. Liu, X.-P. Wang, L. Cao, *J. Nucl. Mater.* **508**, 107 (2018).

[13] J.-P. Bacher, C. Benvenuti, P. Chiggiato, M.-P. Reinert, S. Sgobba, A.-M. Brass, *J. Vacuum Sci. Technol. A* **21**, 167 (2003).

[14] O. Todoshchenko, Y. Yagodzinskyy, H. Hänninen, *Defect Diffus. Forum* **344**, 71 (2013).

[15] T. Hanna, H. Hiramatsu, I. Sakaguchi, H. Hosono, *Rev. Sci. Instrum.* **88**, 053103 (2017).

[16] S.C. Chang, T. Lin, T. Li, *J. Nanomater.* **2014**, 690498 (2014).

[17] M. Bruel, B. Aspar, B. Charlet, C. Maleville, T. Poumeyrol, A. Soubie, A.J. Auberton-Herve, J.M. Lamure, T. Barge, in: *1995 IEEE International SOI Conf. Proc.*, 1995, p. 178.

[18] A. Baudrant, *Silicon Technologies: Ion Implantation and Thermal Treatment* John Wiley & Sons, 2013.

[19] R. Kögler, A. Peeva, A. Lebedev, M. Posselt, W. Skorupa, G. Oezelt, H. Hutter, M. Behar, *J. Appl. Phys.* **94**, 3834 (2003).

[20] E. Oliviero, M.L. David, M.F. Beaufort, J.F. Barbot, A. van Veen, *Appl. Phys. Lett.* **81**, 4201 (2002).

[21] F. Corni, G. Calzolari, F. Gambetta, C. Nobili, R. Tonini, M. Zapparoli, *Mater. Sci. Eng. B* **71**, 207 (2000).

[22] G.F. Cerofolini, G. Calzolari, F. Corni, S. Frabboni, C. Nobili, G. Ottaviani, R. Tonini, *Phys. Rev. B* **61**, 10183 (2000).

[23] S. Godey, E. Ntsoenzok, T. Sauvage, A. van Veen, F. Labohm, M.F. Beaufort, J.F. Barbot, *Mater. Sci. Eng. B* **73**, 54 (2000).

[24] P. Desgardin, M.-F. Barthe, E. Ntsoenzok, C.-L. Liu, *Appl. Surf. Sci.* **252**, 3231 (2006).

[25] M. Turek, A. Droździel, K. Pyszniak, A. Wójtowicz, D. Mączka, Y. Yuschkevich, Y. Vaganov, J. Żuk, *Acta. Phys. Pol. A* **128**, 849 (2015).

[26] W.M. Lau, I. Bello, L.J. Huang, X. Feng, M. Vos, I.V. Mitchell, *J. Appl. Phys.* **74**, 7105 (1993).

[27] A. Filius, A. van Veen, K.R. Bijkerk, J.H. Evans, *Radiat. Eff.* **108**, 1 (1989).

[28] R. Hanada, S. Saito, S. Nagata, S. Yamaguchi, T. Shinozuka, I. Fujioka, *Mater. Sci. Forum* **196–201**, 1375 (1995).

[29] A. Drozdziel, A. Wojtowicz, M. Turek, K. Pyszniak, D. Mączka, B. Slowinski, Y.V. Yushkevich, J. Zuk, *Acta Phys. Pol. A* **125**, 1400 (2014).

[30] M. Werner, J.A. van den Berg, D.G. Armour et al., *Appl. Phys. Lett.* **86**, 151904 (2005).

[31] P.F. Barbieri, R. Landers, F.C. Marques, *Appl. Phys. Lett.* **90**, 164104 (2007).

[32] M. Turek, A. Droździel, K. Pyszniak, A. Wójtowicz, Y. Vaganov, *Przeglad Elektrotechniczny* **94**, 157 (2018).

[33] M. Turek, A. Droździel, A. Wójtowicz, J. Filiks, K. Pyszniak, D. Mączka, Y. Yuschkevich, *Acta Phys. Pol. A* **132**, 249 (2017).

[34] J. Vanhellemont, E. Simoen, *J. Electrochem. Soc.* **154**, H572 (2007).

[35] S. Prucnal, Y. Berencén, M. Wang et al., *Phys. Rev. Appl.* **10**, 064055 (2018).

[36] S. Prucnal, F. Liu, Y. Berencen et al., *Semicond. Sci. Technol.* **31**, 105012 (2016).

[37] S. Prucnal, Y. Berencen, M. Wang et al., *J. Appl. Phys.* **125**, 203105 (2019).

[38] S. Prucnal, J. Żuk, R. Hübner, J. Duan, M. Wang, K. Pyszniak, A. Drozdziel, M. Turek, S. Zhou, *Materials* **13**, 1408 (2020).

[39] M-L. David, K. Alix, F. Pailloux, V. Mauchamp, M. Couillard, G.A. Botton, L. Pizzagalli *J. Appl. Phys.* **115**, 123508 (2014).

[40] F. Yang, X.-X. Zhang, T.-C. Ye, S.-L. Zhuang *J. Electrochem. Soc.* **158**, H1233 (2011).

[41] M. Turek, A. Droździel, K. Pyszniak, S. Prucnal, J. Żuk, Yu. Vaganov, *Acta Phys. Pol. A* **136**, 285 (2019).

[42] M. Turek, A. Droździel, K. Pyszniak, S. Prucnal, J. Żuk, Yu. Vaganov, *Przeglad Elektrotechniczny* **96**, 126 (2020).

[43] F. Corni, C. Nobili, G. Ottaviani, R. Tonini, G. Calzolari, G.F. Cerofolini, G. Queirolo, *Phys. Rev. B* **56**, 7331 (1997).

[44] P.A. Redhead, *Vacuum* **12**, 203 (1962).